JOURNAL OF MAGNETIC RESONANCE, Series B 104, 143–147 (1994)

Standing Waves in Uniform Water Phantoms

PAUL S. TOFTS

NMR Research Group, Institute of Neurology, National Hospital for Neurology and Neurosurgery, Queen Square, London WC1N 3BG, United Kingdom

Received August 13, 1993; revised October 18, 1993

To measure and correct nonuniformity in magnetic resonance images, large cylindrical water phantoms have traditionally been used. Above about 0.5 T, the large dielectric constant of water causes standing wave effects in water phantoms, giving a nonuniform RF field inside the phantom, even when the external field is uniform. The field and signal inside a nonconducting long cylinder are calculated for coils with circular and linear polarization, as a function of phantom diameter and field strength. At 1.5 T, the signal drops by 10% at the edge of a 9.5 cm diameter water cylinder. Oil phantoms are preferred, since the dielectric constant is lower (80 for water, about 5 for oil). At 1.5 T, the signal drops 10% at the edge of a 38 cm oil cylinder. A previous expression (G. H. Glover *et al., J. Magn. Reson.* **64**, 255, 1985) for the internal field and signal for a coil with circular polarization is in error.

Large uniform phantoms are required to map the nonuniform sensitivity of the RF coils in magnetic resonance imagers (*1–3*). If the phantom is made of water, which has a large dielectric constant ($\epsilon = 80$), dielectric standing waves increase the RF magnetic field inside the phantom (*4*), producing an irregular, nonuniform response even in a uniform excitation field. The effect increases with the size of the phantom and with frequency. An alternative is to use an oil phantom (*3, 5*), with $\epsilon = 3$–5. The phantoms are usually cylindrical in shape, with the axis pointing along the static field B_0. The RF field inside a long uniform nonconducting cylinder and the signal from it are both calculated theoretically in this paper. From this a prediction is made of the maximum-size water phantom that will be acceptable for measuring nonuniformity. Two errors in a previous paper on the subject (*4*) are reported.

The field inside a long cylinder, exposed to a field perpendicular to the axis, is (*6*)

$$B_{ry} = \frac{2B_{1y}}{I_0(Ka)} \frac{I_1(Kr)}{Kr} \sin\phi;$$

$$B_{\phi y} = \frac{2B_{1y}}{I_0(Ka)}\left[I_0(Kr) - \frac{I_1(Kr)}{Kr}\right]\cos\phi, \qquad [1]$$

where I_0 and I_1 are modified Bessel functions, a is the radius of the cylinder, B_{1y} is the external field applied along the y axis (see Fig. 1), and B_{ry}, $B_{\phi y}$ are the radial and tangential components of the resulting internal field. K is the complex wave number (*6*), which reduces, in a nonconducting medium, to

$$K = ik; \quad k = \omega(\epsilon\epsilon_0\mu_0)^{1/2}, \qquad [2]$$

where ω is the angular frequency, ϵ is the dielectric constant or relative permittivity, ϵ_0, μ_0 are the permittivity and permeability of free space (8.854×10^{-12} F m^{-1} and $4\pi \times 10^{-7}$ H m^{-1}, respectively), and k is the imaginary part of K that gives rise to phase shifts but no power losses. As an example, at 1.5 T (64 MHz), $k = 1.34$ m^{-1} in free space ($\epsilon = 1$) and k = 12.0 m^{-1} in water ($\epsilon = 80$). The wavelength in air at 1.5 T (4.7 m) is much larger than the width of any object likely to be imaged; however, the effect of the high dielectric constant of water is to reduce the wavelength by a factor of $\sqrt{\epsilon} \approx 9$ in water, to 0.52 m, which is comparable with the width of human subjects.

The maximum value of the real part of K, k_r, that gives rise to power loss in a conducting medium is next estimated for a water phantom that may have been doped to reduce its relaxation times, but to which no NaCl has been added

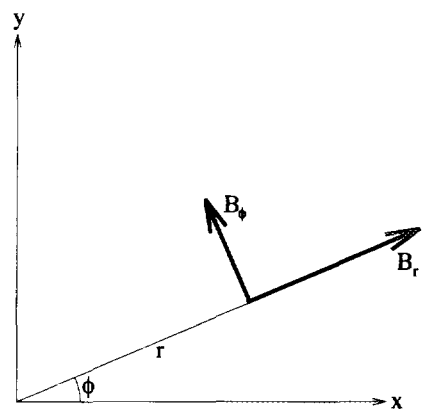

FIG. 1. Coordinate system.

1064-1866/94 $6.00

to explicitly increase its conductivity. At low values of conductivity σ, $k_r \approx (\sigma/2)(\mu_0/\epsilon\epsilon_0)^{1/2}$ (6). T_1 can be shortened to 500 ms with ~2 mM $CuSO_4$ at 0.5 T (7), or ~3 mM $CuSO_4$ at 1.5 T (8). $MnCl_2$ has a higher relaxivity, and consequently much lower concentrations are required (7). An upper limit to the conductivity of $CuSO_4$ solutions can be obtained by comparison with NaCl solutions, which have higher conductivity (the ions are smaller and more mobile). The conductivity of 3 mM NaCl solution is $30 \times 10^{-3}\ \Omega^{-1}\ m^{-1}$ (9); putting this into the above expression for k_r gives $k_r \leq 0.63\ m^{-1}$. This is 5% of k and can safely be ignored. Thus water, even when doped, can be considered nonconducting, and the dielectric standing wave effects will dominate any penetration (skin depth) effect.

In a nonconducting medium, Eq. [1] reduces to

$$B_{ry} = \frac{2B_{1y}}{J_0(ka)}\frac{J_1(kr)}{kr}\sin\phi;$$

$$B_{\phi y} = \frac{2B_{1y}}{J_0(ka)}\left[J_0(kr) - \frac{J_1(kr)}{kr}\right]\cos\phi, \qquad [3]$$

where J_0, J_1 are (unmodified) Bessel functions, and the relations $I_0(iz) = J_0(z)$, $I_1(iz) = iJ_1(z)$ have been used. Similarly the internal field caused by an external field B_{1x} along the x axis is

$$B_{rx} = \frac{2B_{1x}}{J_0(ka)}\frac{J_1(kr)}{kr}\cos\phi;$$

$$B_{\phi x} = -\frac{2B_{1x}}{J_0(ka)}\left[J_0(kr) - \frac{J_1(kr)}{kr}\right]\sin\phi \qquad [4]$$

(this is obtained by transforming ϕ to $\phi + \pi/2$ in Eq. [3]). Transforming to Cartesian coordinates ($B_x = B_r\cos\phi - B_\phi\sin\phi$; $B_y = B_r\sin\phi + B_\phi\cos\phi$), the internal field caused by an external field in the x direction B_{1x} is

$$B_{xx} = \frac{B_{1x}}{J_0(ka)}\left\{J_0(kr) + \left[\frac{2J_1(kr)}{kr} - J_0(kr)\right]\cos 2\phi\right\}$$

$$B_{yx} = \frac{B_{1x}}{J_0(ka)}\left[\frac{2J_1(kr)}{kr} - J_0(kr)\right]\sin 2\phi \qquad [5]$$

and the field caused by an an external field in the y direction B_{1y} is

$$B_{xy} = \frac{B_{1y}}{J_0(ka)}\left[\frac{2J_1(kr)}{kr} - J_0(kr)\right]\sin 2\phi$$

$$B_{yy} = \frac{B_{1y}}{J_0(ka)}\left\{J_0(kr) - \left[\frac{2J_1(kr)}{kr} - J_0(kr)\right]\cos 2\phi\right\}, \qquad [6]$$

in agreement with a previous result (4).

A circularly polarized (CP) external field, rotating in an anticlockwise ($+\omega$) direction, is represented by $B_{1x} = B_1\cos\omega t$, $B_{1y} = B_1\sin\omega t$. Suppose that this component gives rise to the NMR signal. The total field inside a cylinder exposed to such a field is obtained from Eqs. [5] and [6] and can be expressed as the sum of fields rotating in the $+\omega$ and $-\omega$ directions,

$$B_{x(CP)} = B_{+\omega}\cos(\omega t) + B_{-\omega}\cos(-\omega t + 2\phi)$$

$$B_{y(CP)} = B_{+\omega}\sin(\omega t) + B_{-\omega}\sin(-\omega t + 2\phi) \qquad [7]$$

where

$$B_{+\omega} = \frac{B_1}{J_0(ka)}J_0(kr);$$

$$B_{-\omega} = \frac{B_1}{J_0(ka)}\left[\frac{2J_1(kr)}{kr} - J_0(kr)\right]. \qquad [8]$$

At low fields ($\omega \to 0$; hence, from Eq. [2], $k \to 0$), $J_0(ka) \to 1$, $J_1(kr)/kr \to 0.5$, $J_0(kr) \to 1$; the rotating ($+\omega$) component becomes equal to the external field, the counterrotating ($-\omega$) component becomes zero, and the total field equals the external field, as expected:

$$B_{+\omega} \to B_1; \quad B_{-\omega} \to 0;$$

$$B_{x(CP)} \to B_1\cos(\omega t); \; B_{y(CP)} \to B_1\sin(\omega t). \qquad [9]$$

As kr becomes significant, the rotating component decreases, while the counterrotating component increases in size from zero. The presence of a counterrotating component is perhaps surprising, since the externally applied field is all in the opposite ($+\omega$) direction. It implies that a small signal could be detected using the coil polarized in the counterrotating direction, increasing with kr. $B_{+\omega}$ and $B_{-\omega}$ are shown in Fig. 2, normalized to the value at the center of the cylinder [$B_1/J_0(ka)$]. Note that this central value is larger than the external field; it has been "magnified" by a factor $1/J_0(ka)$. As ka increases, $J_0(ka)$ decreases, and at $ka = 2.405$ (for example, a 40 cm diameter water cylinder at 1.5 T), $J_0(ka) = 0$, and the model predicts an infinitely large internal field.

In a linearly polarized (LP) field along the x axis ($B_{1x} = B_1\cos\omega t$, $B_{1y} = 0$), the internal field is given by Eq. [5] and is in agreement with Glover *et al.*, (4). Thus the internal field is parallel to the external one (i.e., $B_{yx} = 0$) along the x or y axis ($\phi = 0$ or $\pi/2$) and also near the center of the cylinder [as $kr \to 0$, $2J_1(kr)/(kr) - J_0(kr) \to 0$]. Along a radius parallel to the applied field, the amplitude of the internal field is (setting $\phi = 0$ for B_{xx} in Eq. [5])

$$B_{\parallel} = \frac{2B_1}{J_0(ka)}\frac{J_1(kr)}{kr}, \qquad [10]$$

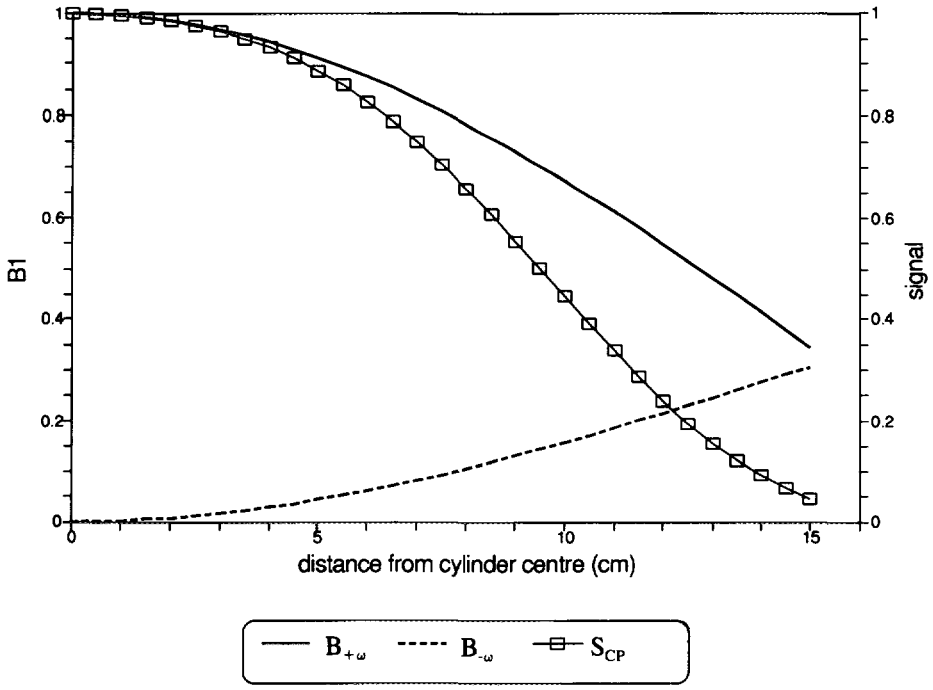

FIG. 2. The rotating field $B_{+\omega}$ (Eq. [8]), counterrotating field $B_{-\omega}$ (Eq. [8]), and signal S_{CP} (Eq. [13]) in a long uniform cylinder of water at 1.5 T (64 MHz) inside a circularly polarized coil. The field values are normalized to the value at the center of the cylinder $[B_1/J_0(ka)]$; the signal is normalized to that from the center of the cylinder when the tip angles of a spin-echo sequence have been correctly set for the center.

while along a radius perpendicular to the applied field it is (setting $\phi = \pi/2$ for B_{xx})

$$B_\perp = \frac{2B_1}{J_0(ka)}\left[J_0(kr) - \frac{J_1(kr)}{kr}\right]. \qquad [11]$$

These functions are shown in Fig. 3, normalized to the field at the center of the cylinder $[B_1/J_0(ka)]$.

The transverse magnetization M_{xy} after a θ–2θ sequence is proportional to $\sin^3\theta$ (*4*). For a spin-echo sequence that has been set correctly for the centre of the cylinder (i.e., $\theta = \pi/2$ at the center), the transverse magnetization a distance r from the center is reduced by the standing-wave effect:

$$M_{xy}(r) = M_{xy}(0)\sin^3\left[\frac{\pi}{2}\frac{B_{+\omega}(r)}{B_{+\omega}(0)}\right]$$

$$= M_{xy}(0)\sin^3\left[\frac{\pi}{2}J_0(kr)\right]. \qquad [12]$$

The receive sensitivity is proportional to $B_{+\omega}$, by the reciprocity theorem (*10*), so the signal from a circularly polarized coil is

$$S_{CP} = S_0\frac{B_{+\omega}(r)}{B_{+\omega}(0)}\frac{M_{xy}(r)}{M_{xy}(0)} = S_0 J_0(kr)\sin^3\left[\frac{\pi}{2}J_0(kr)\right], \qquad [13]$$

where S_0 is the signal from the center of the cylinder. This drop off in signal relative to that at the center depends on r, the distance from the center, but is independent of a, the cylinder radius, and is plotted in Fig. 2. For a linearly polarized coil, using Eqs. [10] and [11], the signal drops off as

$$S_{LP\parallel} = S_0\frac{2J_1(kr)}{kr}\sin^3\left[\pi\frac{J_1(kr)}{kr}\right]$$

$$S_{LP\perp} = S_0\,2\left[J_0(kr) - \frac{J_1(kr)}{kr}\right]\sin^3\left\{\pi\left[J_0(kr) - \frac{J_1(kr)}{kr}\right]\right\}. \qquad [14]$$

This is plotted in Fig. 3.

In designing uniform phantoms to measure and correct spatial nonuniformity in the receiver coil (*1–3*), the dielectric standing-wave effect should not add significant nonuniformity to the signal from the phantom. In other words, in a uniform RF field the signal from the edge of the phantom should not be significantly lower than that from the center. Using Eq. [13] for the circular polarization signal, at the edge of a small cylinder ($ka \to 0$), the signal is

$$S_{CP} \approx S_0\{1 - \tfrac{1}{4}(ka)^2 + O[(ka)^4]\cdots\}, \qquad [15]$$

where $J_0(z)$ has been expanded as $1 - z^2/4 + O(z^4)$. For a linearly polarized coil (Eq. [14]), the signal is

$$S_{LP\parallel} \approx S_0\{1 - \tfrac{1}{8}(ka)^2 + O[(ka)^4]\}$$
$$S_{LP\perp} \approx S_0\{1 - \tfrac{3}{8}(ka)^2 + O[(ka)^4]\}, \quad [16]$$

where $J_1(z)$ has been expanded as $z/2 - z^3/16 + O(z^5)$. The drop in signal in the direction perpendicular to the applied field is three times more than that in the parallel direction. For both polarizations, the term in $(ka)^2$ comes from the drop in receive sensitivity; the drop in transmission sensitivity (i.e., the $\sin^3$ term) does not contribute, since this is at a maximum. Thus the signal reduction at the edge of the cylinder increases quadratically with field and with cylinder size and linearly with dielectric constant ($(ka)^2 \propto \omega^2 a^2 \epsilon$; Eq. [2]).

The maximum-size water phantom that can be used for uniformity measurements at a particular field can be predicted, given the maximum acceptable decrease in signal relative to that at the center. Table 1 shows some results, using Eqs. [13] and [14] ($S_{LP\perp}$). At 1.5 T in a circularly polarized coil, a water phantom can be only 4.6 cm in diameter before standing-wave effects cause 2% nonuniformity; for oil ($\epsilon = 5$), the size can be increased to 18.4 cm before nonuniformity reaches 2%. The validity of the small-cylinder approximations (eqs. [15] and [16]) is strengthened by their ability to predict the nonuniformity values in Table 1. For all the combinations of cylinder size, field, and polarization shown in Table 1 that give 2% nonuniformity, the small-cylinder approximations give 1.9% and hence are good.

TABLE 1

The Maximum-Diameter Long Cylindrical Phantom That Can be Used if Nonuniformity (NU) Is Not to Exceed a Particular Amount for Water ($\epsilon = 80$) and Oil ($\epsilon = 5$)

Field (T)		Maximum-diameter water cylinder (cm)			Maximum-diameter oil cylinder (cm)		
		2% NU	5% NU	10% NU	2% NU	5% NU	10% NU
0.5	CP[a]	13.8	21.0	28.5	55.1	84.1	114.0
	LP[a]	11.3	17.1	23.2	45.0	68.6	92.8
1.5	CP	4.6	7.0	9.5	18.4	28.0	38.0
	LP	3.7	5.7	7.7	15.0	22.9	30.9
4.7	CP	1.5	2.2	3.0	5.9	8.9	12.1
	LP	1.2	1.8	2.5	4.8	7.3	9.9

Note. The maximum diameter scales inversely with field, enabling estimates to be made for other fields.

[a] CP, circular polarization; LP, linear polarization.

Explicit expressions for the spatial variation of the signal in a uniform long cylindrical phantom have been derived in this paper, under the assumption that the external field is uniform. This theory has been compared with data from

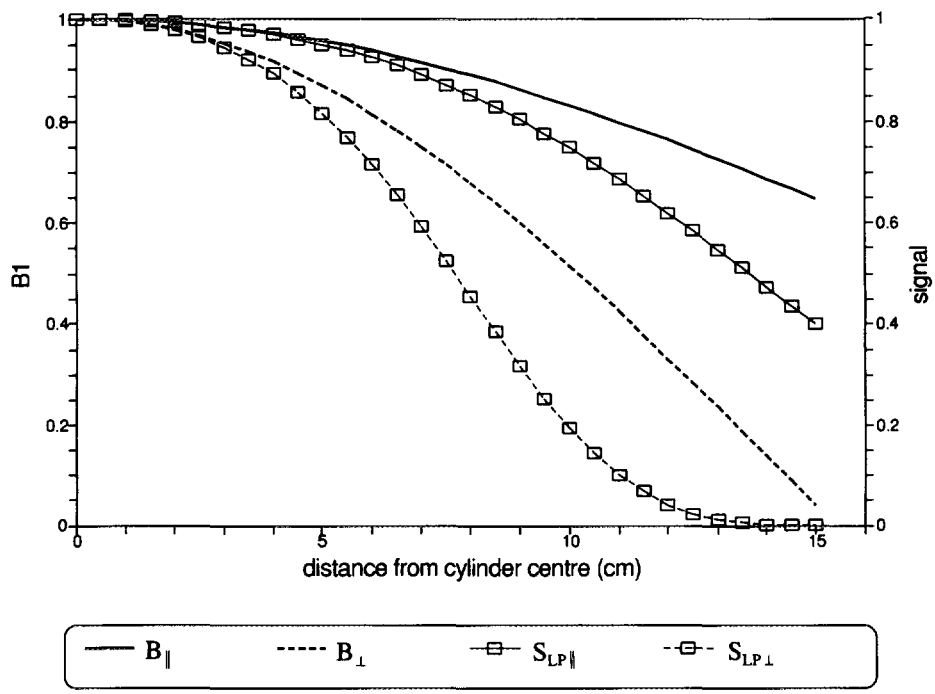

FIG. 3. The field along a line parallel ($B_\parallel$) and perpendicular ($B_\perp$) to the external field (Eqs. [10] and [11]) and signal ($S_{LP\parallel}$, $S_{LP\perp}$; Eq. [14]) in a long uniform cylinder of water at 1.5 T (64 MHz) inside a linearly polarized coil. The field values are normalized to the value at the center of the cylinder [$B_1/J_0(ka)$]; the signal is normalized to that from the center of the cylinder when the tip angles of a spin-echo sequence have been correctly set for the center.

cylinders with lengths about 1.5 times the diameter [(*5*) and private communications from A. Simmons and G. Barker). Images in a large circularly polarized coil at 1.5 T showed good agreement; the signal fell to 10% of its central value at a diameter of 8.0 cm, compared to the predicted value of 9.5 cm (Table 1). In a linearly polarized coil at 4.7 T, the drop off in the direction perpendicular to the field was more rapid than that in the direction parallel, as predicted (Fig. 3); the signal dropped to 10% of its value over a diameter of 1.6 cm, compared to the predicted value of 2.5 cm (Table 1). This discrepancy could have been caused by the phantom being short, or by it being closely coupled to the coil (thus destroying the uniformity of the external RF field).

The use of a uniform nonconducting phantom is primarily aimed at measuring nonuniformity in the response of the radiofrequency transmit and receive coils. Note that the dielectric standing-wave effect *increases* B_1 at the center of the object and is independent of conductivity (provided it is small), while RF penetration effects, caused by conduction in the object, *reduce* B_1 at the center of the object. At high fields and in large objects, a nonconducting phantom may not give a realistic representation of the B_1 distribution in the object. The human body is a complex collection of tissues with differing conductivities and permittivities, separated by relatively insulating membranes, which is extremely hard to model and to represent with a realistic phantom. However, measurements in this laboratory show that in the head, at 1.5 T, dielectric and conductivity effects are small (*5*). This suggests that the heterogeneity of the head structures prevents standing waves from forming, even though they are large in a water phantom of the same size (Table 1). If a realistic conducting phantom is attempted, it cannot be made of water or the standing-wave effects will be large and unrealistic. Possible alternatives are to use oil (although it is hard to see how this could be made conducting), or to fragment the water into small compartments, as it is in the body. Nonconducting phantoms, although not always completely realistic, are easy to design and construct and in this laboratory have an important place in understanding and correcting RF coil nonuniformity in images of the brain, optic nerve, and spinal cord at 1.5 T (*3, 5*).

The previous work by Glover *et al.* (*4*) appears to have two errors. First, from their Eq. [11], in a circularly polarized field, the magnitude of the rotating field in the $+\omega$ direction (defined by them as "the rotation sense of nuclear precession") is $B_+ = [B_1/J_0(ka)][2J_1(kr)/kr - J_0(kr)]$ and in the $-\omega$ direction is $B_- = [B_1/J_0(ka)]J_0(kr)$. This is the reverse of the calculations presented above (Eq. [8]) and fails the tests that at low fields, as $k \to 0$, B_+ should tend toward the external field (B_1) and B_- should tend toward zero. Second, they claim that, although the transmit field is B_+, the receive sensitivity is proportional to B_- (not B_+). This appears to contradict the reciprocity theorem (*10*) and again fails the test of $k \to 0$, implying that either the transmit field or the receive sensitivity vanishes at low field. The theory presented by Bottomley and Andrew (*11*) is for a cylinder with its axis parallel to the applied (external) RF field and cannot be used here.

ACKNOWLEDGMENT

I am grateful to Dr. Gareth Barker for critically reading this manuscript.

REFERENCES

1. B. R. Condon, J. Patterson, D. Wyper, A. Jenkins, and D. M. Hadley, *Br. J. Radiol.* **60,** 83 (1987).
2. D. A. G. Wicks, G. Barker, and P. S. Tofts, *Magn. Reson. Imaging* **11,** 183 (1993).
3. P. S. Tofts, G. J. Barker, D. A. G. Wicks, D. MacManus, A. Simmons, and D. H. Miller, Abstracts of the Society of Magnetic Resonance in Medicine, 11th Annual Meeting, Berlin, Vol. 2, p. 4241, 1992.
4. G. H. Glover, C. E. Hayes, N. J. Pelc, W. A. Edelstein, O. M. Mueller, H. R. Hart, C. J. Hardy, M. O'Donnell, and W. D. Barber, *J. Magn. Reson.* **64,** 255 (1985).
5. A. Simmons, P. S. Tofts, G. J. Barker, D. A. G. Wicks, and S. R. Arridge, Abstracts of the Society of Magnetic Resonance in Medicine, 11th Annual Meeting, Berlin, Vol. 2, p. 4240, 1992.
6. P. Mansfield and P. G. Morris, "Advances in Magnetic Resonance," Suppl. 2, pp. 185–186, Academic Press, New York, 1982.
7. G. Johnson, I. E. C. Ormerod, D. Barnes, P. S. Tofts, and D. MacManus, *Br. J. Radiol.* **60,** 143 (1987).
8. P. S. Tofts, B. Shuter, and J. M. Pope, *Magn. Reson. Imaging* **11,** 125 (1993).
9. R. C. Weast and M. J. Astle (Eds.), "CRC Handbook of Chemistry and Physics," 63rd ed. p. D-277, CRC Press, Boca Raton, Florida, 1982.
10. D. I. Hoult and R. E. Richards, *J. Magn. Reson.* **24,** 71 (1976).
11. P. A. Bottomley and E. R. Andrew, *Phys. Med. Biol.* **23,** 630 (1978).